THE JOURNAL OF PHYSICAL CHEMISTRY B

Article

pubs.acs.org/JPCB

Reactions of Methanesulfonic Acid with Amines and Ammonia as a Source of New Particles in Air

Haihan Chen, Mychel E. Varner, R. Benny Gerber,* and Barbara J. Finlayson-Pitts*

Department of Chemistry, University of California, Irvine, California 92697, United States

Supporting Information

ABSTRACT: New particle formation (NPF) from gaseous precursors as a significant source of aerosol needs to be better understood to accurately predict the impacts on visibility, climate change, and human health. While ternary nucleation of sulfuric acid, amines/NH_3, and water is recognized as a significant driver for NPF, increasing evidence suggests a contribution from methanesulfonic acid (MSA) and amines under certain conditions. Here we report the formation of particles 2.5−10 nm in diameter from the reactions of MSA with methylamine (MA), dimethylamine (DMA), and NH_3 at reaction times of 2.3−7.8 s in a flow reactor and compare these particles with those previously reported to be formed from reaction with trimethylamine (TMA). The effects of water vapor and concentrations of gaseous precursors on the particle number concentration and particle size were studied. The presence of water significantly enhances particle formation and growth. Under similar experimental conditions, particle number concentrations decrease in the order MA ≫ TMA ≈ DMA ≫ NH_3, where NH_3 is 2−3 orders of magnitude less efficient than DMA. Quantum chemical calculations of likely intermediate clusters were carried out to provide insights into the role of water and the different capacities of amines/NH_3 in particle formation. Both gas-phase basicity and hydrogen-bonding capacity of amines/NH_3 contribute to the potential for particles to form and grow. Our results indicate that, although amines typically have concentrations 1−3 orders of magnitude lower than that of NH_3 in the atmosphere, they still play an important role in driving NPF.

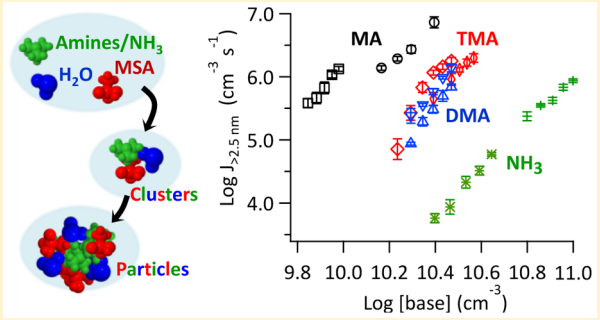

INTRODUCTION

Atmospheric particles have well-known deleterious effects on human health[1,2] and visibility.[3−5] Those particles can globally affect radiative forcing and climate by absorbing and scattering solar radiation as well as by acting as cloud condensation nuclei (CCN) to change cloud coverage and properties.[6−8] However, great uncertainties remain in the mechanisms of formation of atmospheric particles, and these preclude accurate assessment of the impacts of atmospheric particles on human health, visibility, and climate.[9] New particle formation (NPF) from gas-to-particle conversion represents a significant source of atmospheric particles[10,11] and contributes up to half of global CCN.[8,12] Understanding the potential species driving NPF and the underlying mechanisms is therefore critical for prediction and control of climate change.[9,10]

Sulfuric acid (H_2SO_4) formed from SO_2 oxidation in air has been well recognized as a key species driving NPF.[13−15] The reaction of H_2SO_4 with ammonia (NH_3) and amines represents the initial step in gas-to-particle conversion to form small clusters,[10,11] which can further grow into detectable size particles in the atmosphere. Low-volatility, high-molecular-weight organic compounds are likely also involved.[16−20] Although ternary nucleation of H_2SO_4−NH_3−H_2O has been shown to enhance particle formation by orders of magnitude compared to binary nucleation of H_2SO_4−H_2O,[21−26] it is not sufficient to explain particle formation in the atmosphere.[25] Amines can play a more important role in NPF,[24,26−32] possibly due to the stronger bonds they form with H_2SO_4 compared to NH_3.[27] Laboratory experiments have demonstrated that amines are more effective in forming particles with H_2SO_4.[24,26,28−30,32] Field studies have shown that aminium salts are widely present in ambient particles,[31,33−35] and NPF is correlated with the presence of amines.[36,37] In addition, amines have been found to effectively displace NH_3 in ammonium bisulfate clusters/particles,[38−41] with a close-to-collision-limited rate for small clusters.[38,39] Thus, aminium salts are likely to be present even if ammonium salts are initially formed.

Ammonia and amines are emitted from a wide range of sources, including biological processes in the ocean, animal husbandry, industrial operations, fuel and biomass burning, and agricultural activities.[42] The concentration of gas-phase amines in the atmosphere is typically at least one order of magnitude smaller than that of NH_3, but this may increase with their use in CO_2 capture and storage as the technology becomes more widely adopted.[42−45]

Special Issue: Bruce C. Garrett Festschrift

Received: July 31, 2015
Revised: September 17, 2015
Published: September 17, 2015

DOI: 10.1021/acs.jpcb.5b07433
J. Phys. Chem. B 2016, 120, 1526−1536

Methanesulfonic acid (MSA, $MeSO_3H$) that is commonly detected in ambient particles contributes to NPF along with H_2SO_4.[33,34,46−52] MSA is formed along with SO_2 (H_2SO_4 precursor) from the oxidation of organosulfur compounds that originate from biological processes, biomass burning, industrial operations, and agricultural activities.[53−57] Atmospheric gas-phase MSA concentrations are typically in the range of $\sim10^5$−10^7 molecules cm^{-3}, about ∼10−100% of those of H_2SO_4.[58,59] The contribution of MSA to NPF is expected to become relatively more important with implementation of stricter environmental regulations on SO_2 emissions.[60]

Binary nucleation of MSA−H_2O was reported to be much less efficient than that of H_2SO_4−H_2O.[50,52,61−64] However, previous studies from this laboratory showed that trimethylamine (TMA, Me_3N) and dimethylamine (DMA, Me_2NH) promote particle formation from MSA in the presence of water vapor.[50,52] These studies suggested that water not only is involved in particle growth but also participates in the formation of the initial clusters.[50,52]

The objectives of this study are to investigate the effect of water on NPF and growth from MSA with ammonia and a series of amines including methylamine (MA, $MeNH_2$) and DMA, and to compare their capacities in NPF with previously reported TMA.[50] We conducted comprehensive experiments on the reaction of MSA with amines/NH_3 over a range of experimental conditions and at reaction times of 2.3−7.8 s. The structures and thermodynamic properties of likely intermediate clusters were predicted using a quantum chemical approach. Comparison to the previous studies of TMA[50,52] provides insight into the relative contributions of NH_3 and amines in NPF and into the molecular factors that determine the efficiency of these reactions.

EXPERIMENTAL METHODS

Figure S1 in the Supporting Information shows a schematic of the flow reactor, which is made of borosilicate glass and was designed to study the early stages, ∼2.3−32 s, of reaction (time includes 1.9 s in the sampling line). The flow reactor has been well characterized and tested previously.[50,51] Briefly, it is comprised of a major section that has a diameter of 7.6 cm and a length of 1.3 m, with end-caps at both ends to accommodate inlets and outlets. The major section is water-jacketed for temperature control. The upstream end-cap holds two hollow glass ring inlets (Figure S1, ring A and ring B) that are perforated with 36 evenly spaced 0.05 cm holes to disperse gases. Two sets of perforated hollow spokes are fitted to two movable concentric glass tubes and guided into the reactor from the upstream end-cap to serve as the other two inlets (Figure S1, spokes C and spokes D). Gas precursors and particles are sampled from a stainless steel sampling tube that is guided into the flow reactor by the downstream end-cap. Only part of the gas/particle flow is sampled through the sampling tube, and the majority of the flow is vented through a 0.5 in. glass port at the downstream end-cap.

Prior to each experiment, the flow reactor was cleaned with Nanopure water (>18.0 MΩ cm; Model 7146; Thermo Scientific) and dried with purified air with the water jacket kept at ∼70 °C. In all experiments, the mixture of purified air and MSA flow was introduced from the spokes C at a total flow of 2 slpm (standard liter per minute at 25 °C and 101.32 kPa), and the mixture of purified air and the selected amines/NH_3 from the spokes D at a total flow of 1 slpm. Dry/humidified air at a total flow of 14 slpm was introduced from the upstream ring inlets (ring A and ring B) to make the total flow in the flow reactor 17 slpm. Thus, MSA was mixed with water vapor before reacting with the specific amines/NH_3 for experiments under humid conditions. All experiments were performed at ambient temperature. Because of wall losses of MSA, the gas flow of MSA was first introduced into the flow reactor to passivate the walls for 2−3 days. The gas flow of the selected amines/NH_3 was then introduced to initiate particle formation. Particle formation and growth as a function of time were monitored by adjusting the distance between the sampling tube and the spokes inlet D. A previously determined conversion factor (0.14 s cm^{-1}) was used to convert the distance to reaction times.[51]

All of the flows were controlled by high-precision mass flow controllers (Alicat or MKS), and were checked with a flow meter (Gilibrator 2; Sensidyne) prior to each experiment. Dry air was further purified through a purge gas generator (model 75-62; Parker Balston), carbon/alumina media (Perma Pure, LLC), and a 0.1 μm filter (DIF-N70; Headline Filters). Humid air was achieved by passing a portion of the dry air through a water bubbler filled with Nanopure water. The relative humidity (RH) was monitored with a RH probe (model HMT338; Vaisala) at the downstream end of the reactor. The gas-phase MSA flow was generated by passing dry purified air over liquid MSA (99.0%, Fluka) contained in a trap. The gas-phase amines or ammonia were added into the system from gas tanks (1−10 ppm in N_2, Airgas) without further purification.

To determine the concentration of gas-phase MSA, the gas flow out of the MSA trap was first passed through a 0.45 μm Durapore filter (Millex-HV) for 5−15 min for collection. The collected MSA was extracted with 10 mL of Nanopure water, and then the extract was analyzed using ultra-performance liquid chromatography coupled with tandem mass spectrometry (UPLC-MS/MS, Waters). The concentrations of MA, DMA, and NH_3 were determined as previously described.[65] Briefly, the amines/NH_3 from the source were collected for 20−120 min using a high-concentration cartridge that contains a weak cation exchange resin, extracted with 10 mL of 0.1 M oxalic acid (Fluka), and analyzed with ion chromatography (Metrohm). The measured concentrations of ammonia and the amines were typically lower than values provided by the manufacturers. The analysis also confirmed that no significant contaminant of other amines or NH_3 was present in the selected amine/NH_3 (<0.1% of the specific base) flows. The initial concentrations of MSA and amines/NH_3 in the flow reactor were calculated on the basis of the measured concentrations at the sources and the total gas flow in the flow reactor. As a result, the initial concentrations may actually be lower than those reported here due to potential wall losses in the flow reactor inlets and the flow reactor itself.

Dry and humidified diluent air in the flow reactor was also collected from the sampling tube using a low-concentration cartridge[65] to examine possible amines and ammonia present as contaminants in the diluents air, and the concentrations of amines and ammonia were all lower than the 10 ppt detection limit.

Particle size distributions were measured using a scanning mobility particle sizer (SMPS) that consists of an electrostatic classifier (model 3080; TSI), a nano-differential mobility analyzer (model 3085; TSI), and a butanol-based condensation particle counter (model 3776; TSI). The 50% cutoff size of the SMPS for sucrose particles is reported by the manufacturer to

DOI: 10.1021/acs.jpcb.5b07433
J. Phys. Chem. B 2016, 120, 1526−1536

be ~2.5 nm. All particle diameters reported here are geometric mean mobility diameters obtained from the SMPS.

THEORETICAL METHODS

To examine the effect of water and differences in the nature of the amine on the stability of intermediate clusters, structures and thermodynamic parameters were determined for clusters consisting of one or two acid/amine molecules and up to two water molecules. For $(MSA)_2 \cdot (amine)_2 \cdot (H_2O)_n$ [n = 0, 1, or 2], as well as their parent clusters and molecules, optimizations and frequency calculations at the B3LYP-D3/6-31+G(d,p) level of theory, including dispersion correction,[66] with electronic energies calculated at the latter level of theory, provided the structures and thermodynamic values. Test calculations indicate that use of the B3LYP-D3/6-31+G(d,p) geometries and harmonic frequencies leads to differences of ~1 kcal mol^{-1} (and often less) for ΔH and ΔG values computed using RIMP2/aug-cc-pV(D+d)Z, which was used previously for MSA-amine systems.[52] Bork et al.[67] tested several DFT and *ab initio* methods against an experimentally determined ΔG value for the acetonitrile-HCl hydrogen-bonded complex and found that MP2 and B3LYP-D3 predictions were within the experimental range. For the smaller $(MSA) \cdot (amine) \cdot (H_2O)_n$ [n = 0 or 1] clusters, optimizations and frequency calculations at the RIMP2/aug-cc-pV(D+d)Z level of theory with electronic energies calculated at the RIMP2/aug-cc-pV(D+d)Z level of theory were employed. All calculations were carried out with the Turbomole program package.[68,69] A detailed description of the theoretical methods is included in the Supporting Information.

RESULTS AND DISCUSSION

Experimental Results. The effect of water on NPF and growth was first investigated for selected amines/NH_3. The initial concentrations of the precursors and water vapor were kept at similar levels as the nature of the base was varied in order to make direct comparisons (Table 1). However, in the case of NH_3, the concentrations of the base increased in order to form detectable particles (Table 1).

Figure 1 shows particle size distributions as a function of reaction time for MA (Figure 1a), DMA (Figure 1b), and NH_3 (Figure 1c) either under dry conditions or with added water vapor. Clearly, particle formation and growth are much more favorable when water is present. An enhancement effect of water vapor on particle formation has also been reported in previous H_2SO_4-amines studies.[24,28,29,70,71] In some cases in this study, there are spikes in the size distributions of particles below the SMPS cutoff of 2.5 nm at short reaction times (Figure 1). This suggests the presence of smaller particles or clusters <2.5 nm in size that can grow into the detectable size range at longer reaction times. Preliminary data obtained with a particle size magnifier (model A10; Airmodus) which has a cutoff size of ~1.4 nm for ammonium sulfate particles confirms the presence of particles smaller than 2.5 nm in size. As indicated in the previous study,[50] we did not observe particle formation from MSA−H_2O in the absence of amines/NH_3, indicating that ammonia and amines present at ppt levels as contaminants from the water and air used in the experiment do not lead to particle formation.

Further comparisons of particle number concentrations and diameters are shown in Figure 2. Similar plots for TMA reported earlier[50] are shown in Figure S2 in the Supporting Information for comparison. In the case of MA (Figure 2a), the number concentration and diameter at a reaction time of 7.8 s are larger by factors of 5 and 2, respectively, at 45% RH compared to those under dry conditions. Particle diameter (Figure 2a, lower panel) at 45% RH slowly levels off with time, indicating the depletion of gas-phase precursors. For example, if the density of the bulk of the particles is taken as 1.3 g cm^{-3},[72] the composition as 1:1:1 MSA:MA:H_2O, and the measured volume concentration of particles using SMPS of 3.4×10^9 nm^3 cm^{-3} at 7.8 s, the number of MSA molecules in the particle phase is calculated to be 2×10^{10} MSA per cm^3 of air. Even if particles are mainly composed of water with a particle composition of 1:1:10 MSA:MA:H_2O, the number of MSA molecules tied up in the particle phase would be 1×10^{10} MSA per cm^3 of air. The initial concentration of MSA is 5×10^{10} cm^{-3} based on the MSA exiting the trap, but this is an upper limit as there are likely losses on the inlet lines and the flow reactor. Thus, the estimated number of MSA molecules tied up in particles is similar in magnitude to the initial number of MSA in the gas phase, suggesting that most of the gaseous precursors are tied up in particles after 5 s. Most of the formation of new particles (Figure 2a, upper panel) has occurred by the first measurement time of 2.3 s. The particle number concentration decreases after 3.8 s because of a combination of depletion of gas-phase precursors, coagulation, and wall losses. Compared to MA as well as TMA reported earlier,[50] DMA is much less effective in forming particles with MSA in the absence of water (Figures 1b and 2b), with particle number concentrations lower by 2−3 orders of magnitude under similar conditions.

When water is present, the particle number concentrations for the MA, DMA, and TMA reactions at 7.8 s are of the same order of magnitude (~10^7 cm^{-3}) (Figures 2 and S2). However, particle formation is slower initially in the cases of DMA and TMA, suggesting that there is more of a kinetic limitation compared to the MA reaction.

The effect of water was further investigated by monitoring particle formation and growth as a function of RH, while MSA and the amine concentrations were held constant. Figure 3 shows that particle number concentrations increase as the RH increases for all bases, MA (Figure 3a, upper panel), DMA (Figure 3b, upper panel), and NH_3 (Figure 3c, upper panel). Increasing RH also promotes particle growth in the cases of MA (Figure 3a, lower panel) and NH_3 (Figure 3c, lower panel),

Table 1. Concentrations of Gaseous Precursors and Relative Humidity Used in Experiments to Investigate the Effect of Water

base	RH (%)	[MSA][a] (ppb)	[base][a] (ppb)
MA	<2	2.1	2.5
	45		
DMA	<2	1.8	2.5
	46		
TMA[b]	<2	1.8	2.5
	48		
NH_3	<2	1.9	18
	42		

[a]Measured from the sources, representing upper limits for the concentrations given the possible losses in flow reactor inlets and the flow reactor itself. [b]Data from ref 50.

DOI: 10.1021/acs.jpcb.5b07433
J. Phys. Chem. B 2016, 120, 1526−1536

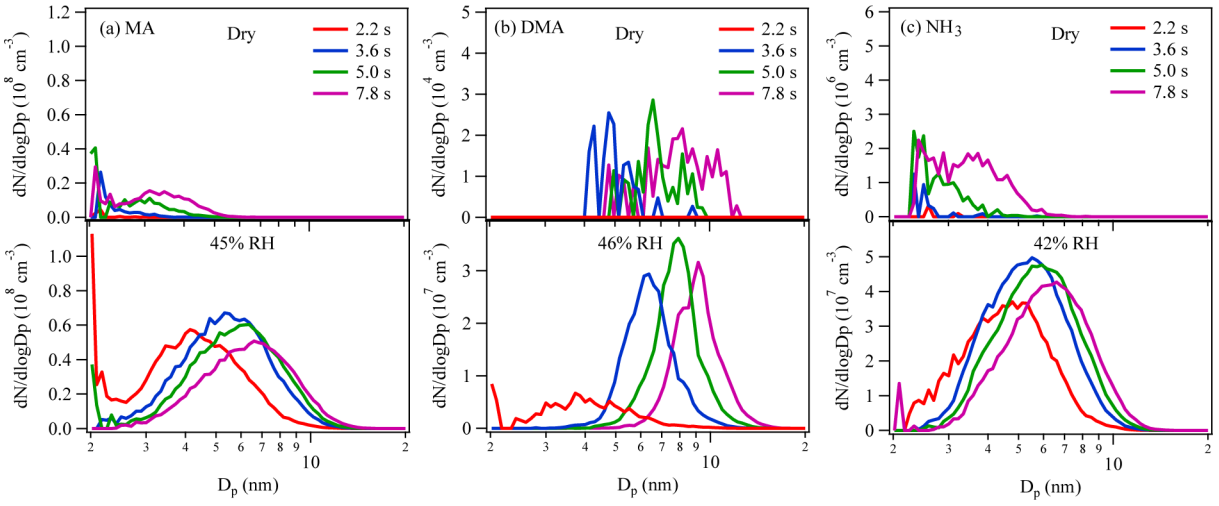

Figure 1. Size distributions of particles measured by SMPS at different reaction times from the reactions of (a) 2.1 ppb MSA with 2.5 ppb MA; (b) 1.8 ppb MSA with 2.5 ppb DMA; and (c) 1.9 ppb MSA with 18 ppb NH_3. Size distributions under dry and humid conditions are shown in the upper and lower panels, respectively. Note the difference vertical scales for DMA and NH_3 in the absence compared to the presence of water. Size distributions were also measured at reaction times of 2.9, 3.3, and 6.4 s but are not shown in the plots for clarity.

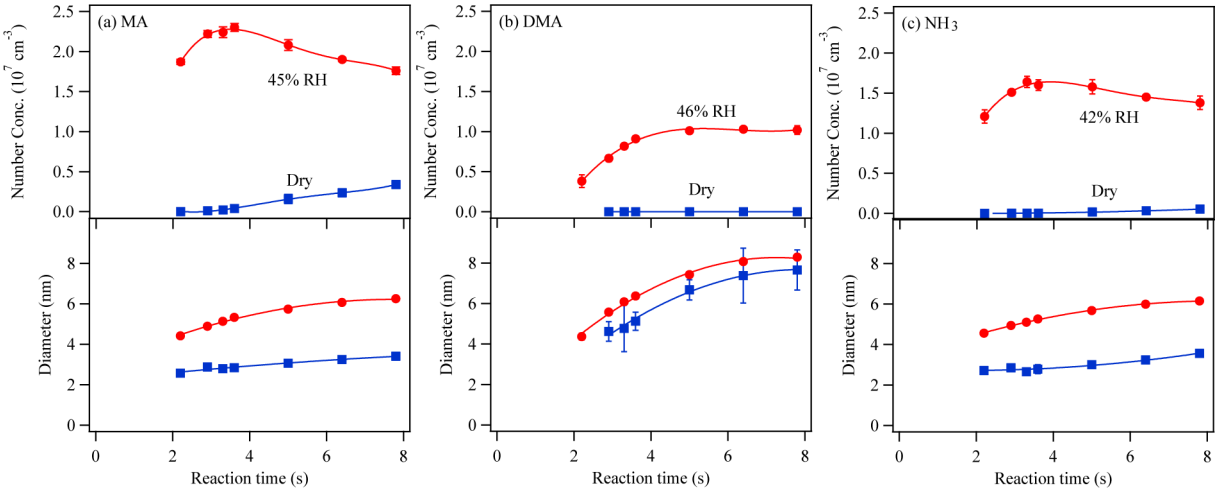

Figure 2. Number concentrations (upper panel) and diameters (lower panel) of particles as a function of reaction time under dry (blue filled squares) and humid conditions (red filled circles). Particles were measured by SMPS from the reactions of (a) 2.1 ppb MSA with 2.5 ppb MA; (b) 1.8 ppb MSA with 2.5 ppb DMA; and (c) 1.9 ppb MSA with 18 ppb NH_3. The lines between data points are drawn as guides to the eye. Uncertainties represent two standard deviations from triplicate SMPS measurements and lie within the symbols in some cases.

but has relatively little effect on the growth of MSA−DMA particles.

The data in Figure 3 clearly show a strong dependence of particle formation on the water vapor concentration. In the context of classical nucleation theory, the slope of a log−log plot of the initial formation rate of detectable particles ($J_{>2.5\ nm}$) against the gas-phase water concentration can provide information on the number of water molecules in the critical cluster,[73] although this is somewhat controversial.[74] Alternatively, the overall reaction order can reflect the rate-determining steps in the formation and growth of the initial clusters; for example, if the MSA dihydrate was the key reactive species, a second order dependence on water could result.

The different shapes of the curves at short reaction times in the top panel of Figure 3 result in significant uncertainty in determining $J_{>2.5\ nm}$. Recognizing this caveat, as a first approach, values of $J_{>2.5\ nm}$ were estimated using the 2.3−3.6 s regions in Figure 3. The resulting log−log plot of $J_{>2.5\ nm}$ as a function of water vapor concentration for all of the amines/NH_3 investigated is shown in Figure 4. Experiments were repeated at least twice for each base. A similar dependence found for the MSA−TMA−H_2O system[50] is included. The slopes obtained for different amines/NH_3 are in the range of 1.3−2.3, indicating that the particle formation rate is approximately overall second order with respect to water.

Experiments were also carried out in which the concentration of MA was varied in the presence of excess MSA (Figure 5). (Experiments under the reverse conditions of excess MA resulted in particle formation rates that were too rapid to be followed at short reaction times.) Both number concentrations and size increase with increasing concentrations of MA. The induction period (Figure 5) that does not appear at higher concentrations of MSA and MA (Figure 2a) suggests that longer reaction times are required for small clusters to grow into detectable size particles at lower concentrations of gas precursors.

DOI: 10.1021/acs.jpcb.5b07433
J. Phys. Chem. B 2016, 120, 1526−1536

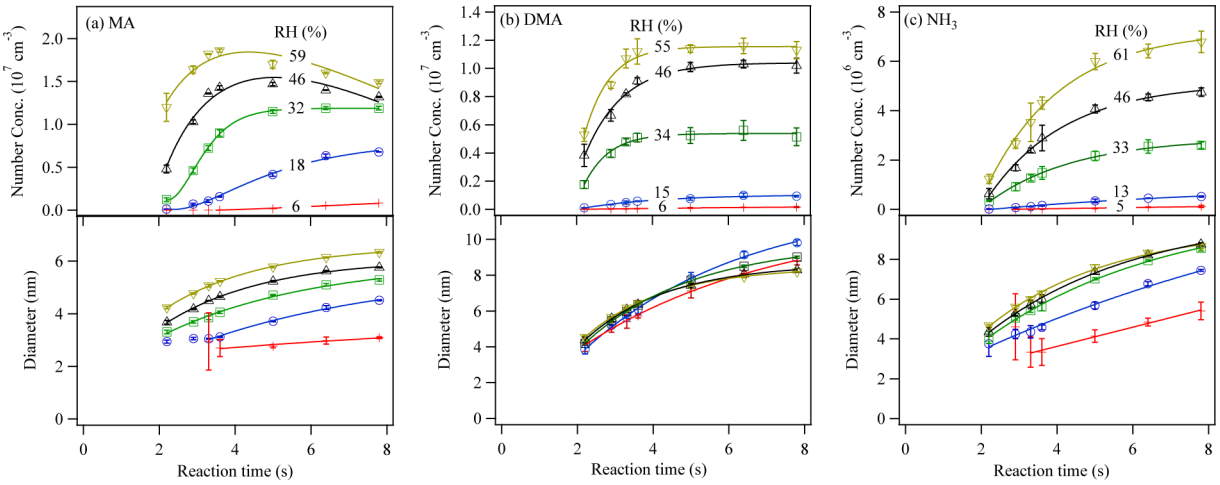

Figure 3. Number concentrations (upper panel) and diameters (lower panel) of particles from the reactions of MSA with selected bases as a function of reaction time at various RH. Particles are measured by SMPS from the reactions of (a) 2.1 ppb MSA with 0.8 ppb MA; (b) 1.8 ppb MSA with 2.5 ppb DMA; and (c) 2.0 ppb MSA with 5.6 ppb NH_3. The lines between data points are drawn as guides to the eye. Uncertainties represent two standard deviations from triplicate SMPS measurements and lie within the symbols in some cases. Measurements of the diameters have high uncertainties at short reaction times due to the experimental challenges of detecting low particle numbers, and those data have been disregarded in drawing lines.

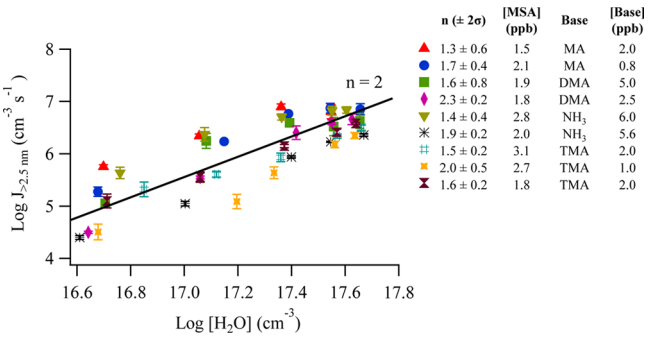

Figure 4. Particle formation rates as a function of H_2O observed in the MSA−base−H_2O system. Error bars represent two standard deviations and lie within the symbols in some cases. The basic species are MA, DMA, TMA, and NH_3. Experiments were repeated at least twice under varied concentrations of MSA, base, and H_2O for each type of basic species. The power dependency ($n \pm 2\sigma$) and the concentrations of MSA and the base for each experiment are shown. The TMA data are from ref 50.

Experiments were also performed for particle formation from the reactions of MSA with MA, DMA, TMA or NH_3 at a constant concentration of MSA at 1.7 ppb at 55% RH. A comparison of $J_{>2.5\ nm}$ for different amines/NH_3 is shown in Figure 6. Results from two separate experiments for each base are in good agreement. The different basic species show different abilities in forming particles with MSA. Consistent with previous studies in the H_2SO_4−amines/NH_3 system,[24,26−30] amines are much more effective than NH_3 in promoting particle formation from MSA. Of the three amines studied here, MA is by far the most effective, followed by TMA and DMA.

Theoretical Calculations. Both gas-phase basicity and hydrogen-bonding capacity can contribute to the potential for particles to form and grow. With increasing gas-phase basicity, the reaction with MSA is more exothermic. With increasing hydrogen-bonding capacity, the sites for addition of molecules from the gas phase increase in number. However, neither gas-phase basicity, which increases with the number of methyl groups for the series MA < DMA < TMA, nor hydrogen-bonding capacity, which decreases with the number of methyl

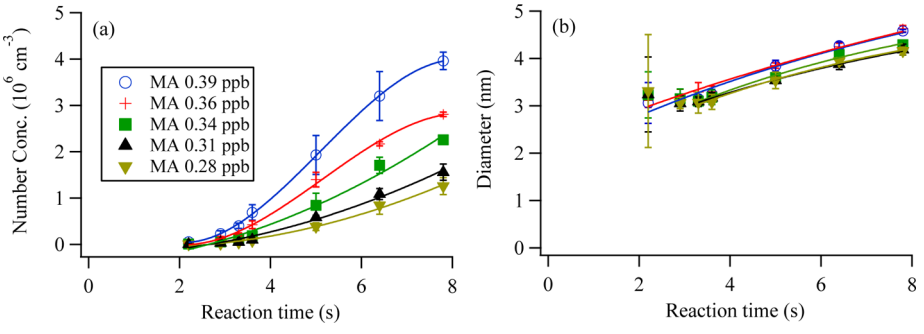

Figure 5. (a) Number concentrations and (b) diameters of particles measured by SMPS from the reaction of 1.0 ppb MSA with variable concentrations of MA as a function of reaction time at 55% RH. The lines between data points are drawn to as guides to the eye. Uncertainties represent two standard deviations from triplicate SMPS measurements and lie within the symbols in some cases. Measurements of the diameters have high uncertainties at short reaction times due to the experimental challenges of detecting low particle numbers, and those data have been disregarded in drawing lines.

DOI: 10.1021/acs.jpcb.5b07433
J. Phys. Chem. B 2016, 120, 1526−1536

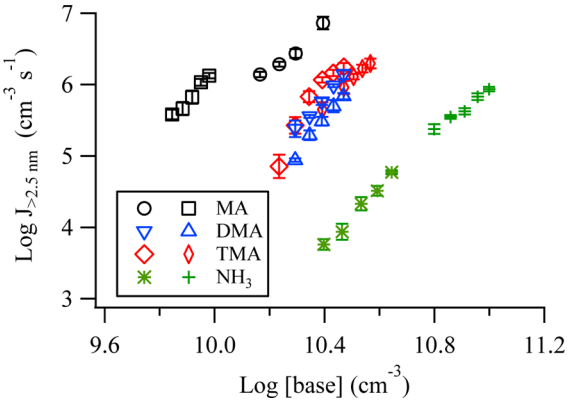

Figure 6. Comparison of particle formation rates ($J_{>2.5\ nm}$) for MSA with the basic species, i.e., MA, DMA, TMA, and NH_3, at ~55% RH. The initial concentration of MSA is 1.7 ppb. Two separate experiments were performed for each base, and the data are represented as symbols with different shapes.

groups for the series MA > DMA > TMA, alone can explain the observed lack of particle formation for DMA relative to both TMA and MA under dry conditions. Calculations for alternating addition of acid and base molecules to the initial acid−base ion pair were carried out in an attempt to identify differences in the growth mechanisms that would explain the differences in particle formation rates observed experimentally for the series of amines.

The stability of the cluster formed from addition of MSA to the initial acid−amine ion pair is similar for MA and DMA (MA: ΔH = −29 kcal mol^{-1}, ΔG = −15 kcal mol^{-1}; DMA: ΔH = −29 kcal mol^{-1}, ΔG = −16 kcal mol^{-1}). MSA addition to the TMA ion pair ($MeSO_3^-$)·(Me_3NH^+) occurs through hydrogen bonding of the acidic −OH group to an −SO group of the anion (Figure 7a). This leads to a somewhat weaker interaction compared to the MA and DMA cases where an additional hydrogen bond to an available −NH group is formed (Figures 8a and 9a), but MSA is still strongly bound to the TMA ion pair (ΔH = −25 kcal mol^{-1}, ΔG = −12 kcal mol^{-1}). As MSA addition is favorable in all cases, and not less favorable for DMA where there is limited particle formation under dry conditions, we move to the next step: amine addition to the $(MSA)_2$·(amine) cluster.

Structures for $(MSA)_2$·$(TMA)_2$ isomers are also included in Figure 7. Addition of a second TMA molecule may form an initial intermediate (Figure 7b) which is energetically stable, ΔH = −5 kcal mol^{-1} (ΔG = +4 kcal mol^{-1}). This intermediate (Figure 7b) may then isomerize to the significantly more stable ($MeSO_3^-$)$_2$·(Me_3NH^+)$_2$ cluster (Figure 7c), ΔH = −21 kcal mol^{-1} (ΔG = −9 kcal mol^{-1}) relative to $(MSA)_2$·(TMA) + TMA.

The addition of MA to a $(MSA)_2$·(MA) cluster to form a stable ($MeSO_3^-$)$_2$·($MeNH_3^+$)$_2$ (Figure 8c) may proceed through a weakly bound complex (Figure 8b) similar to that of TMA (Figure 7b). The binding enthalpy of this complex is similar to the TMA case, ΔH = −5 kcal mol^{-1} (ΔG = +5 kcal mol^{-1}). However, in the case of MA an alternate route for cluster growth may facilitate particle formation under dry conditions. The $(MSA)_2$·(MA) cluster consists of a ($MeSO_3^-$)·($MeNH_3^+$) ion pair similar to the TMA cluster, but with the additional −NH groups of MA, the MSA molecule is hydrogen-bonded to both the anion and cation (Figure 8a). The $MeNH_3^+$

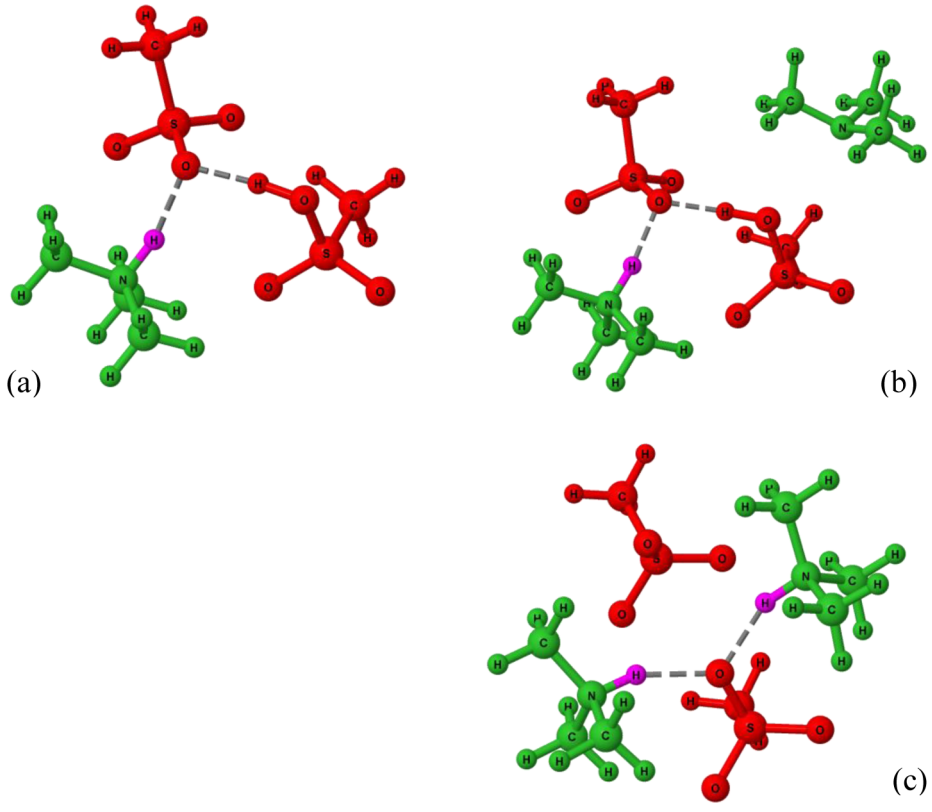

Figure 7. Structures for $(MSA)_2$·(TMA) and isomers of $(MSA)_2$·$(TMA)_2$: (a) $(MSA)_2$·(TMA), (b) the initial complex for addition of TMA at the hydrogen-bonded MSA of $(MSA)_2$·(TMA), and (c) the double ion pair cluster of $(MSA)_2$·$(TMA)_2$. Red represents MSA, green the amine.

DOI: 10.1021/acs.jpcb.5b07433
J. Phys. Chem. B 2016, 120, 1526−1536

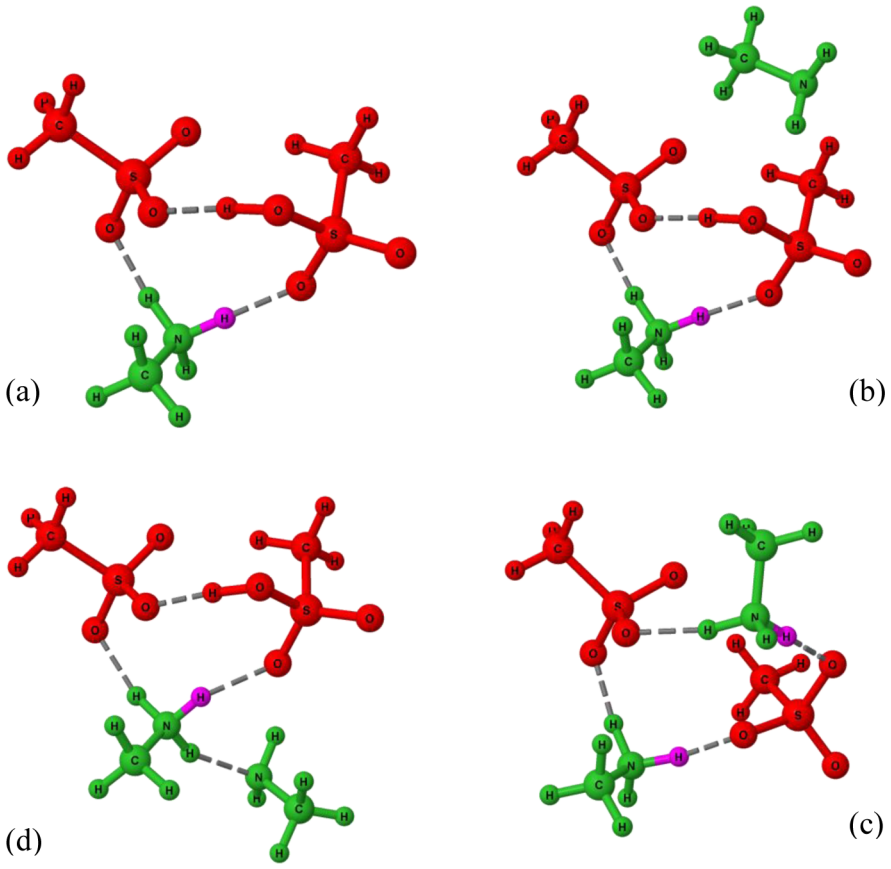

Figure 8. Structures for $(MSA)_2{\cdot}(MA)$ and isomers of $(MSA)_2{\cdot}(MA)_2$: (a) $(MSA)_2{\cdot}(MA)$, (b) the initial complex for addition of MA at the hydrogen-bonded MSA of $(MSA)_2{\cdot}(MA)$, (c) the double ion pair cluster of $(MSA)_2{\cdot}(MA)_2$, and (d) the initial complex for addition of MA at the −NH group of the cation of $(MSA)_2{\cdot}(MA)$. Red represents MSA, green the amine.

cation has a remaining hydrogen-bonding site available for addition of the second MA molecule from the gas phase. Addition of the second amine at the cation (Figure 8d) forms a more stable intermediate (ΔH = −11 kcal mol^{-1} and ΔG = −2 kcal mol^{-1}) than at the hydrogen-bonded MSA (Figure 8b: ΔH = −5 kcal mol^{-1}, ΔG = +5 kcal mol^{-1}).

Binding of DMA to a $(MSA)_2{\cdot}(DMA)$ cluster (Figure 9a) to form $(MSA)_2{\cdot}(DMA)_2$ (Figure 9c) either at the hydrogen-bonded MSA (Figure 9b: ΔH = −8 kcal mol^{-1}, ΔG = +2 kcal mol^{-1}) or at the cation (Figure 9d: ΔH = −13 kcal mol^{-1}, ΔG = −2 kcal mol^{-1}), is slightly greater than the corresponding MA system. The two routes for cluster growth, addition either at the cation or at the neutral acid molecule, both seem to be feasible for the MSA−DMA system, and potentially more likely based on enthalpies of formation of the complexes. The conclusion from these calculations is that understanding the anomalous dry behavior of DMA will require consideration of intermediates at the level of four or more molecule clusters.

Dawson et al.[72] described structures and binding for $(MSA)_2{\cdot}(MA)_2$, $(MSA)_2{\cdot}(DMA)_2$, and $(MSA)_2{\cdot}(TMA)_2$ clusters, including speculation on the nature of interactions in extended systems. The endothermicity for dissociation of $(MSA)_2{\cdot}(TMA)_2$ to $(MeSO_3^-)(Me_3NH^+)$ ion pairs, ΔH = 24 kcal mol^{-1}, is similar to the exothermicity of TMA addition to $(MSA)_2{\cdot}(TMA)$ presented above. Due to the lack of hydrogen bonds between $(MeSO_3^-)(Me_3NH^+)$ ion pairs, the single ion pair formed on fragmentation may then play a significant role in growing the stabilized clusters to detectable size particles.[50] For comparison, the binding energies of ion pairs in forming $(MSA)_2{\cdot}(MA)_2$ and $(MSA)_2{\cdot}(DMA)_2$ clusters (ΔH = −36 and −37 kcal mol^{-1}, respectively) are close and are significantly larger than the binding energy informing $(MSA)_2{\cdot}(TMA)_2$ due to a cyclic hydrogen-bonding structure between alternating cations and anions.[72] However, the availability of an NH group that is not hydrogen-bonded in the MA cluster may lead to an extended hydrogen-bonding network, an arrangement seen in the crystal structure of ammonium methanesulfonate.[75] While growth of a perfect crystal may not occur in this case, the additional hydrogen-bonding site may play a role in more effectively growing the MSA-MA clusters to detectable sizes even under dry conditions. For DMA, the large binding energy between MSA-DMA ion pairs enhances the formation and stability of $(MSA)_2{\cdot}(DMA)_2$ clusters, so that these double ion pairs may play an important role in growth to detectable particle sizes. Coagulation of two of these larger clusters may exhibit steric effects, whereas growth through single ion pairs for TMA would be less sterically hindered, leading to more rapid formation of detectable particles in the TMA system.

Structures of $(MSA)_2{\cdot}(DMA){\cdot}(H_2O)_2$ and $(MSA)_2{\cdot}(DMA)_2{\cdot}(H_2O)_2$ illustrating how water facilitates amine addition are included in Figure 10. The incorporation of water into the $(MSA)_2{\cdot}(DMA)$ cluster provides hydrogen-bonding sites for initial addition from the gas phase. Addition of DMA to $(MSA)_2{\cdot}(DMA){\cdot}(H_2O)_2$ (Figure 10a) leads directly to a very stable cluster (Figure 10b: ΔH = −27 kcal mol^{-1}, ΔG = −16 kcal mol^{-1}). A weakly bound intermediate, analogous to that of the dry cluster, was not identified in the case of the hydrated clusters.

DOI: 10.1021/acs.jpcb.5b07433
J. Phys. Chem. B 2016, 120, 1526−1536

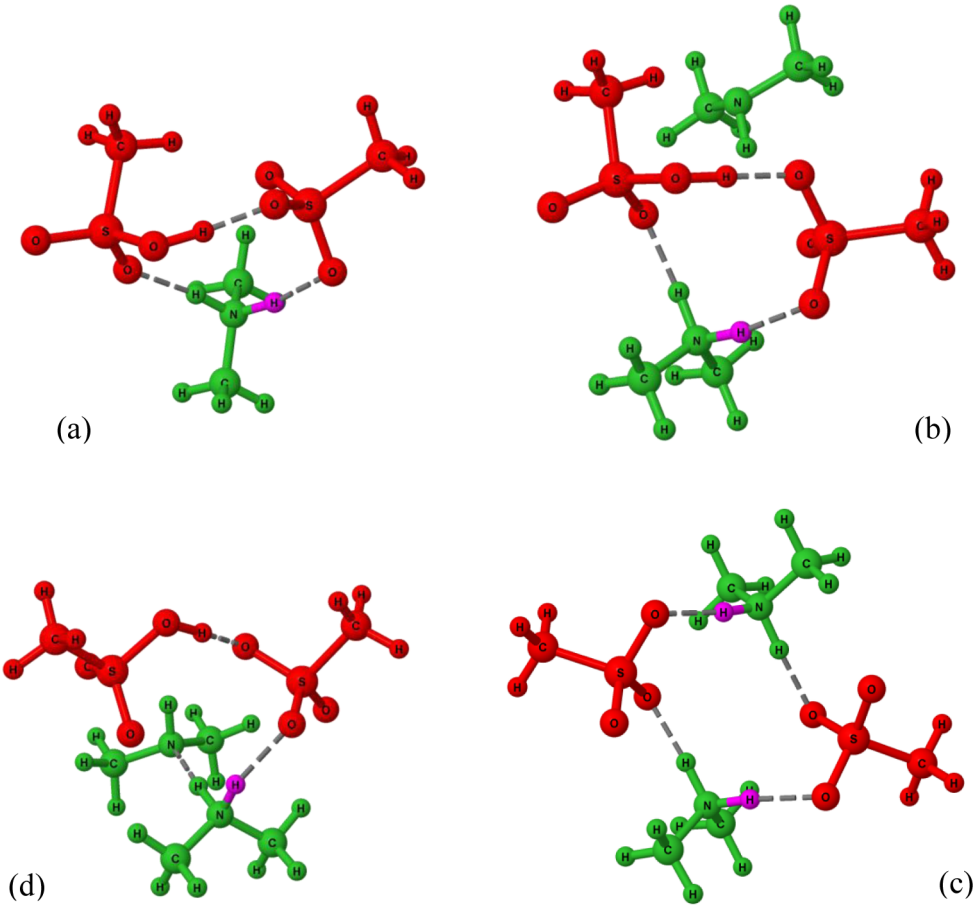

Figure 9. Structures for $(MSA)_2{\cdot}(DMA)$ and isomers of $(MSA)_2{\cdot}(DMA)_2$: (a) $(MSA)_2{\cdot}(DMA)$, (b) the initial complex for addition of DMA to the hydrogen-bonded MSA of $(MSA)_2{\cdot}(DMA)$, (c) the double ion pair cluster of $(MSA)_2{\cdot}(DMA)_2$, and (d) the initial complex for addition of DMA at the −NH group of the cation of $(MSA)_2{\cdot}(DMA)$. Red represents MSA, green the amine.

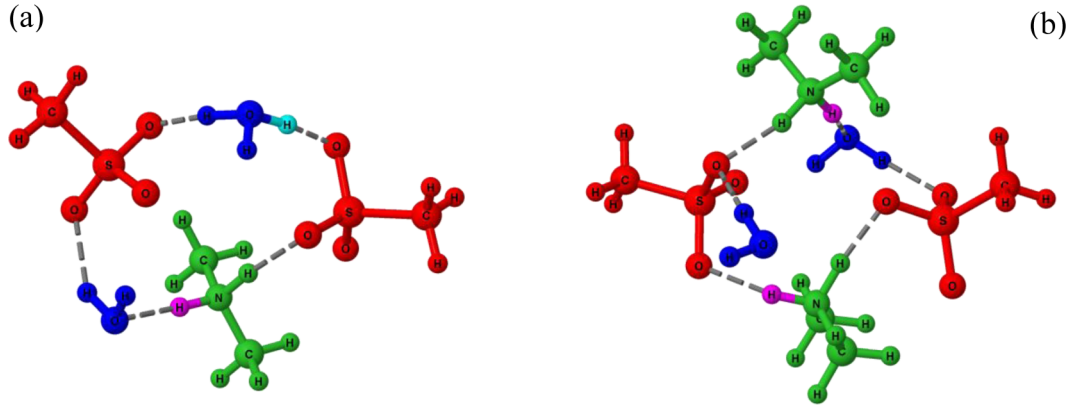

Figure 10. Structures for (a) $(MSA)_2{\cdot}(DMA){\cdot}(H_2O)_2$ and (b) $(MSA)_2{\cdot}(DMA)_2{\cdot}(H_2O)_2$. Red represents MSA, green the amine, blue the H_2O.

The binding of water to the initial ion pair is slightly greater for MA and DMA (ΔH = −15 kcal mol^{-1}, $\Delta G \approx$ −5 kcal mol^{-1}) than for TMA (ΔH = −11 kcal mol^{-1}, $\Delta G \approx$ −2 kcal mol^{-1}). While there is not a significant difference in the binding energy of water to the MA vs DMA ion pair, the MA ion pair has an additional hydrogen-bonding site that may increase the chances of picking up water from the gas phase. If hydrated clusters are formed more quickly or are more stable, and hydration aids cluster growth, this could explain the faster formation of detectable particles from MA (Figure 2a) compared to DMA (Figure 2b) and TMA (Figure S2). The growth of DMA and TMA particles is also significantly faster than the MA particles (Figure 2 and S2). This can be due to (1) a larger contribution of growth from water because of their higher hygroscopicities,[72] (2) a larger molecular volume, and/or (3) smaller particle formation rates so that higher concentrations of gas precursors and small clusters that can contribute to growth are left in the DMA and TMA systems.

It is noteworthy that at essentially the same concentration of MSA (Table 1), NH_3 needs to be at much higher concentrations (18 ppb) than MA, DMA or TMA (2.5 ppb) to form comparable number concentrations of particles (Figure

DOI: 10.1021/acs.jpcb.5b07433
J. Phys. Chem. B 2016, 120, 1526−1536

2c). Clearly, NH_3 is much less effective in particle formation similar to the case of H_2SO_4-amines/NH_3 studies.[24,26−30,32] The formation energies of MSA·NH_3 and MSA·NH_3·H_2O were calculated to be $\Delta H = -14$ kcal mol^{-1} ($\Delta G = -5$ kcal mol^{-1}) and $\Delta H = -26$ kcal mol^{-1} ($\Delta G = -6$ kcal mol^{-1}), respectively, significantly lower than the corresponding clusters of amines (Table 2). The formation of initial clusters is less favorable in the NH_3 system, resulting in less effectiveness in NPF (Figure 6).

Table 2. Formation Energies and Enthalpies for Initial Clusters of MSA with Amines/Ammonia

	MSA·base		MSA·base·H_2O	
base	ΔH (kcal mol^{-1})	ΔG (kcal mol^{-1})	ΔH (kcal mol^{-1})	ΔG (kcal mol^{-1})
MA	−18	−7	−32	−11
DMA	−21	−9	−36	−15
TMA	−22	−12	−34	−14
NH_3	−14	−5	−26	−6

If gas-phase basicity and hydrogen-bonding capacity are the two competing factors in particle formation and growth for the series of amines studied here, the success of MA in forming particles indicates that the hydrogen-bonding capacity of the amine plays a larger role, though the ineffectiveness of ammonia indicates that threshold basicity is required. This differs from the case of sulfuric acid,[29,32] which provides greater hydrogen-bonding capacity, so it is not surprising that the relative effects of amines are different than for MSA.

The conceptual approach taken in this paper involves calculations for small clusters, with extrapolation to likely growth possibilities. Calculations for larger particles are obviously very desirable. One appealing direction is to carry out calculations for crystalline particles, using periodic boundary conditions. As the crystalline salt is likely not the most relevant model for growth of the early-stage clusters and at the disordered surface, and high-level calculations with periodic boundary conditions remain a challenge for systems of this size, this approach was not pursued here, but it is a very interesting direction for the future.

■ ATMOSPHERIC IMPLICATIONS

Particle formation and growth are observed for reactions of MSA with ammonia and three small alkyl amines, MA, DMA, and, as reported earlier,[50] TMA. Thus, the reaction of MSA with ammonia and amines must contribute to NPF in the atmosphere. Consistent with the previous studies,[50,52] water shows a significant enhancement effect on particle formation and growth from MSA. Relative humidity is therefore expected to be a critical factor affecting NPF in the atmosphere.

Similar to previous studies on the H_2SO_4−amines/NH_3 system,[24,26−30] amines are much more effective in forming particles with MSA than ammonia. Different bases show capacities in NPF with MSA in the order of MA ≫ TMA ≈ DMA ≫ NH_3.

While particle formation rates of amines with MSA are about 2−3 orders of magnitude higher than that of ammonia, field measurements in agricultural, ocean, and landfill areas usually show concentrations of amines approximately 1−3 orders of magnitude lower than those of ammonia.[42] Together these indicate that amines, despite having relatively smaller concentrations in the atmosphere, are expected to play a significant role in the initial stages of NPF.

■ ASSOCIATED CONTENT

Supporting Information

The Supporting Information is available free of charge on the ACS Publications website at DOI: 10.1021/acs.jpcb.5b07433.

Figure S1, schematic of the flow reactor; Figure S2, particle formation and growth in the MSA−TMA system; detailed description of the theoretical methods; and Cartesian coordinates and B3LYP-D3/6-31++G** and RIMP2/aug-cc-pV(T+d)Z electronic energies of the structures in Figures 7−10 (PDF)

■ AUTHOR INFORMATION

Corresponding Authors

*For theory, R.B.G.: E-mail bgerber@uci.edu.

*For experiments, B.J.F.-P.: E-mail bjfinlay@uci.edu, phone (949) 824-7670, fax (949) 824-2420.

Notes

The authors declare no competing financial interest.

■ ACKNOWLEDGMENTS

The authors are grateful to the National Science Foundation (grant nos. 0909227 and 1443140) for funding. We thank Metrohm USA for their support and help in ion chromatography analysis. Computational resources include the Greenplanet cluster at University of California, Irvine, the CSC cluster Taito in Helsinki, Finland, and those of the Fritz-Haber Center in Jerusalem, Israel. It is a pleasure to dedicate this paper to Bruce Garrett, whose contributions from molecular interactions with liquid surfaces to nucleation theory and particle growth greatly impacted the study of atmospheric chemistry and have been a major influence on work done at AirUCI. His support of a strong interaction between theory and experiment is one important example.

■ REFERENCES

(1) Pope, C. A., III; Dockery, D. W. Health Effects of Fine Particulate Air Pollution: Lines that Connect. *J. Air Waste Manage. Assoc.* **2006**, *56*, 709−742.

(2) Heal, M. R.; Kumar, P.; Harrison, R. M. Particles, Air Quality, Policy and Health. *Chem. Soc. Rev.* **2012**, *41*, 6606−6630.

(3) Hinds, W. C. *Aerosol Technology: Properties, Behavior and Measurement of Airborne Particles*; John Wiley & Sons Inc.: New York, 1999.

(4) Finlayson-Pitts, B. J.; Pitts, J. N., Jr. *Chemistry of the Upper and Lower Atmosphere: Theory, Experiments, and Applications*; Academic Press: San Diego, 2000.

(5) Seinfeld, J. H.; Pandis, S. N. *Atmospheric Chemistry and Physics: From Air Pollution to Climate Change*; John Wiley & Sons: New York, 2006.

(6) Kerminen, V.-M.; Lihavainen, H.; Komppula, M.; Viisanen, Y.; Kulmala, M. Direct Observational Evidence Linking Atmospheric Aerosol Formation and Cloud Droplet Activation. *Geophys. Res. Lett.* **2005**, *32*, L14803.

(7) Spracklen, D. V.; Carslaw, K. S.; Kulmala, M.; Kerminen, V.-M.; Sihto, S.-L.; Riipinen, I.; Merikanto, J.; Mann, G. W.; Chipperfield, M. P.; Wiedensohler, A.; et al. Contribution of Particle Formation to Global Cloud Condensation Nuclei Concentrations. *Geophys. Res. Lett.* **2008**, *35*, L06808.

(8) Kuang, C.; McMurry, P. H.; McCormick, A. V. Determination of Cloud Condensation Nuclei Production from Measured New Particle Formation Events. *Geophys. Res. Lett.* **2009**, *36*, L09822.

DOI: 10.1021/acs.jpcb.5b07433
J. Phys. Chem. B 2016, 120, 1526−1536

(9) Stocker, T. F.; Dahe, Q.; Plattner, G.-K. *Climate Change 2013: The Physical Science Basis*; Cambridge University Press: Cambridge, UK, 2013.
(10) Zhang, R.; Khalizov, A.; Wang, L.; Hu, M.; Xu, W. Nucleation and Growth of Nanoparticles in the Atmosphere. *Chem. Rev.* **2012**, *112*, 1957−2011.
(11) Kulmala, M.; Vehkamäki, H.; Petäjä, T.; Dal Maso, M.; Lauri, A.; Kerminen, V.-M.; Birmili, W.; McMurry, P. H. Formation and Growth Rates of Ultrafine Atmospheric Particles: A Review of Observations. *J. Aerosol Sci.* **2004**, *35*, 143−176.
(12) Merikanto, J.; Spracklen, D. V.; Mann, G. W.; Pickering, S. J.; Carslaw, K. S. Impact of Nucleation on Global CCN. *Atmos. Chem. Phys.* **2009**, *9*, 8601−8616.
(13) Weber, R. J.; Chen, G.; Davis, D. D.; Mauldin, R. L., III; Tanner, D. J.; Eisele, F. L.; Clarke, A. D.; Thornton, D. C.; Bandy, A. R. Measurements of Enhanced H_2SO_4 and 3−4 nm Particles Near a Frontal Cloud during the First Aerosol Characterization Experiment (ACE 1). *J. Geophys. Res.* **2001**, *106*, 24107−24117.
(14) Weber, R. J.; Marti, J. J.; McMurry, P. H.; Eisele, F. L.; Tanner, D. J.; Jefferson, A. Measured Atmospheric New Particle Formation Rates: Implications for Nulceation Mechanisms. *Chem. Eng. Commun.* **1996**, *151*, 53−64.
(15) Weber, R. J.; Marti, J. J.; McMurry, P. H.; Eisele, F. L.; Tanner, D. J.; Jefferson, A. Measurements of New Particle Formation and Ultrafine Particle Growth Rates at a Clean Continental Site. *J. Geophys. Res.* **1997**, *102*, 4375−4385.
(16) Kulmala, M.; Kontkanen, J.; Junninen, H.; Lehtipalo, K.; Manninen, H. E.; Nieminen, T.; Petaja, T.; Sipila, M.; Schobesberger, S.; Rantala, P.; et al. Direct Observations of Atmospheric Aerosol Nucleation. *Science* **2013**, *339*, 943−946.
(17) Ehn, M.; Thornton, J. A.; Kleist, E.; Sipila, M.; Junninen, H.; Pullinen, I.; Springer, M.; Rubach, F.; Tillmann, R.; Lee, B.; et al. A Large Source of Low-Volatility Secondary Organic Aerosol. *Nature* **2014**, *506*, 476−479.
(18) Donahue, N. M.; Ortega, I. K.; Chuang, W.; Riipinen, I.; Riccobono, F.; Schobesberger, S.; Dommen, J.; Baltensperger, U.; Kulmala, M.; Worsnop, D. R.; et al. How do Organic Vapors Contribute to New-Particle Formation? *Faraday Discuss.* **2013**, *165*, 91−104.
(19) Riccobono, F.; Schobesberger, S.; Scott, C. E.; Dommen, J.; Ortega, I. K.; Rondo, L.; Almeida, J.; Amorim, A.; Bianchi, F.; Breitenlechner, M.; et al. Oxidation Products of Biogenic Emissions Contribute to Nucleation of Atmospheric Particles. *Science* **2014**, *344*, 717−721.
(20) Zhang, R.; Suh, I.; Zhao, J.; Zhang, D.; Fortner, E. C.; Tie, X.; Molina, L. T.; Molina, M. J. Atmospheric New Particle Formation Enhanced by Organic Acids. *Science* **2004**, *304*, 1487−1490.
(21) Ball, S. M.; Hanson, D. R.; Eisele, F. L.; McMurry, P. H. Laboratory Studies of Particle Nucleation: Initial Results for H_2SO_4, H_2O, and NH_3 Vapors. *J. Geophys. Res.* **1999**, *104*, 23709−23718.
(22) Korhonen, P.; Kulmala, M.; Laaksonen, A.; Viisanen, Y.; McGraw, R.; Seinfeld, J. H. Ternary Nucleation of H_2SO_4, NH_3, and H_2O in the Atmosphere. *J. Geophys. Res.* **1999**, *104*, 26349−26353.
(23) Benson, D. R.; Erupe, M. E.; Lee, S.-H. Laboratory-Measured H_2SO_4-H_2O-NH_3 Ternary Homogeneous Nucleation Rates: Initial Observations. *Geophys. Res. Lett.* **2009**, *36*, L15818.
(24) Berndt, T.; Stratmann, F.; Sipilä, M.; Vanhanen, J.; Petäjä, T.; Mikkilä, J.; Grüner, A.; Spindler, G.; Lee Mauldin, R., III; Curtius, J.; et al. Laboratory Study on New Particle Formation from the Reaction OH + SO_2: Influence of Experimental Conditions, H_2O Vapour, NH_3 and the Amine Tert-Butylamine on the Overall Process. *Atmos. Chem. Phys.* **2010**, *10*, 7101−7116.
(25) Kirkby, J.; Curtius, J.; Almeida, J.; Dunne, E.; Duplissy, J.; Ehrhart, S.; Franchin, A.; Gagné, S.; Ickes, L.; Kürten, A.; et al. Role of Sulphuric Acid, Ammonia and Galactic Cosmic Rays in Atmospheric Aerosol Nucleation. *Nature* **2011**, *476*, 429−433.
(26) Zollner, J. H.; Glasoe, W. A.; Panta, B.; Carlson, K. K.; McMurry, P. H.; Hanson, D. R. Sulfuric Acid Nucleation: Power Dependencies, Variation with Relative Humidity, and Effect of Bases. *Atmos. Chem. Phys.* **2012**, *12*, 4399−4411.
(27) Kurtén, T.; Loukonen, V.; Vehkamäki, H.; Kulmala, M. Amines Are Likely to Enhance Neutral and Ion-Induced Sulfuric Acid-Water Nucleation in the Atmosphere More Effectively Than Ammonia. *Atmos. Chem. Phys.* **2008**, *8*, 4095−4103.
(28) Erupe, M. E.; Viggiano, A. A.; Lee, S.-H. The Effect of Trimethylamine on Atmospheric Nucleation Involving H_2SO_4. *Atmos. Chem. Phys.* **2011**, *11*, 4767−4775.
(29) Yu, H.; McGraw, R.; Lee, S.-H. Effects of Amines on Formation of Sub-3 nm Particles and Their Subsequent Growth. *Geophys. Res. Lett.* **2012**, *39*, L02807.
(30) Almeida, J.; Schobesberger, S.; Kürten, A.; Ortega, I. K.; Kupiainen-Määttä, O.; Praplan, A. P.; Adamov, A.; Amorim, A.; Bianchi, F.; Breitenlechner, M.; et al. Molecular Understanding of Sulphuric Acid-Amine Particle Nucleation in the Atmosphere. *Nature* **2013**, *502*, 359−363.
(31) Smith, J. N.; Barsanti, K. C.; Friedli, H. R.; Ehn, M.; Kulmala, M.; Collins, D. R.; Scheckman, J. H.; Williams, B. J.; McMurry, P. H. Observations of Aminium Salts in Atmospheric Nanoparticles and Possible Climatic Implications. *Proc. Natl. Acad. Sci. U. S. A.* **2010**, *107*, 6634−6639.
(32) Glasoe, W. A.; Volz, K.; Panta, B.; Freshour, N.; Bachman, R.; Hanson, D. R.; McMurry, P. H.; Jen, C. Sulfuric Acid Nucleation: An Experimental Study of the Effect of Seven Bases. *J. Geophys. Res. Atmos.* **2015**, *120*, 1933−1950.
(33) Facchini, M. C.; Decesari, S.; Rinaldi, M.; Carbone, C.; Finessi, E.; Mircea, M.; Fuzzi, S.; Moretti, F.; Tagliavini, E.; Ceburnis, D.; et al. Important Source of Marine Secondary Organic Aerosol from Biogenic Amines. *Environ. Sci. Technol.* **2008**, *42*, 9116−9121.
(34) Sorooshian, A.; Padró, L. T.; Nenes, A.; Feingold, G.; McComiskey, A.; Hersey, S. P.; Gates, H.; Jonsson, H. H.; Miller, S. D.; Stephens, G. L.; et al. On the Link Between Ocean Biota Emissions, Aerosol, and Maritime Clouds: Airborne, Ground, and Satellite Measurements Off the Coast of California. *Glob. Biogeochem. Cycle* **2009**, *23*, GB4007.
(35) Pratt, K. A.; Hatch, L. E.; Prather, K. A. Seasonal Volatility Dependence of Ambient Particle Phase Amines. *Environ. Sci. Technol.* **2009**, *43*, 5276−5281.
(36) Freshour, N. A.; Carlson, K. K.; Melka, Y. A.; Hinz, S.; Panta, B.; Hanson, D. R. Amine Permeation Sources Characterized with Acid Neutralization and Sensitivities of an Amine Mass Spectrometer. *Atmos. Meas. Tech.* **2014**, *7*, 3611−3621.
(37) Jen, C. N.; McMurry, P. H.; Hanson, D. R. C. J. D. Stabilization of Sulfuric Acid Dimers by Ammonia, Methylamine, Dimethylamine, and Trimethylamine. *J. Geophys. Res. Atmos.* **2014**, *119*, 7502−7514.
(38) Bzdek, B. R.; Ridge, D. P.; Johnston, M. V. Size-Dependent Reactions of Ammonium Bisulfate Clusters with Dimethylamine. *J. Phys. Chem. A* **2010**, *114*, 11638−11644.
(39) Bzdek, B. R.; Ridge, D. P.; Johnston, M. V. Amine Exchange into Ammonium Bisulfate and Ammonium Nitrate Nuclei. *Atmos. Chem. Phys.* **2010**, *10*, 3495−3503.
(40) Liu, Y.; Han, C.; Liu, C.; Ma, J.; Ma, Q.; He, H. Differences in the Reactivity of Ammonium Salts with Methylamine. *Atmos. Chem. Phys.* **2012**, *12*, 4855−4865.
(41) Qiu, C.; Wang, L.; Lal, V.; Khalizov, A. F.; Zhang, R. Heterogeneous Reactions of Alkylamines with Ammonium Sulfate and Ammonium Bisulfate. *Environ. Sci. Technol.* **2011**, *45*, 4748−4755.
(42) Ge, X.; Wexler, A. S.; Clegg, S. L. Atmospheric Amines − Part I. A review. *Atmos. Environ.* **2011**, *45*, 524−546.
(43) Rochelle, G. T. Amine Scrubbing for CO_2 Capture. *Science* **2009**, *325*, 1652−1654.
(44) Nielsen, C. J.; Herrmann, H.; Weller, C. Atmospheric Chemistry and Environmental Impact of the Use of Amines in Carbon Capture and Storage (CCS). *Chem. Soc. Rev.* **2012**, *41*, 6684−6704.
(45) Qiu, C.; Zhang, R. Multiphase Chemistry of Atmospheric Amines. *Phys. Chem. Chem. Phys.* **2013**, *15*, 5738−5752.
(46) Mäkelä, J. M.; Yli-Koivisto, S.; Hiltunen, V.; Seidl, W.; Swietlicki, E.; Teinilä, K.; Sillanpää, M.; Koponen, I. K.; Paatero, J.; Rosman, K.;

DOI: 10.1021/acs.jpcb.5b07433
J. Phys. Chem. B 2016, 120, 1526−1536

et al. Chemical Composition of Aerosol during Particle Formation Events in Boreal Forest. *Tellus, Ser. B* **2001**, *53*, 380−393.
(47) Hopkins, R. J.; Desyaterik, Y.; Tivanski, A. V.; Zaveri, R. A.; Berkowitz, C. M.; Tyliszczak, T.; Gilles, M. K.; Laskin, A. Chemical Speciation of Sulfur in Marine Cloud Droplets and Particles: Analysis of Individual Particles from the Marine Boundary Layer over the California Current. *J. Geophys. Res.* **2008**, *113*, D04209.
(48) Gaston, C. J.; Pratt, K. A.; Qin, X.; Prather, K. A. Real-time Detection and Mixing State of Methanesulfonate in Single Particles at an Inland Urban Location during a Phytoplankton Bloom. *Environ. Sci. Technol.* **2010**, *44*, 1566−1572.
(49) Zorn, S. R.; Drewnick, F.; Schott, M.; Hoffmann, T.; Borrmann, S. Characterization of the South Atlantic Marine Boundary Layer Aerosol using an Aerodyne Aerosol Mass Spectrometer. *Atmos. Chem. Phys.* **2008**, *8*, 4711−4728.
(50) Chen, H.; Ezell, M. J.; Arquero, K. D.; Varner, M. E.; Dawson, M. L.; Gerber, R. B.; Finlayson-Pitts, B. J. New Particle Formation and Growth from Methanesulfonic Acid, Trimethylamine and Water. *Phys. Chem. Chem. Phys.* **2015**, *17*, 13699−13709.
(51) Ezell, M. J.; Chen, H.; Arquero, K. D.; Finlayson-Pitts, B. J. Aerosol Fast Flow Reactor for Laboratory Studies of New Particle Formation. *J. Aerosol Sci.* **2014**, *78*, 30−40.
(52) Dawson, M. L.; Varner, M. E.; Perraud, V.; Ezell, M. J.; Gerber, R. B.; Finlayson-Pitts, B. J. Simplified Mechanism for New Particle Formation from Methanesulfonic Acid, Amines, and Water via Experiments and Ab Initio Calculations. *Proc. Natl. Acad. Sci. U. S. A.* **2012**, *109*, 18719−18724.
(53) Bates, T. S.; Lamb, B. K.; Guenther, A.; Dignon, J.; Stoiber, R. E. Sulfur Emissions to the Atmosphere from Natural Sourees. *J. Atmos. Chem.* **1992**, *14*, 315−337.
(54) VanderGheynst, J. S.; Cogan, D. J.; DeFelice, P. J.; Gossett, J. M.; Walker, L. P. Effect of Process Management on the Emission of Organosulfur Compounds and Gaseous Antecedents from Composting Processes. *Environ. Sci. Technol.* **1998**, *32*, 3713−3718.
(55) Rosenfeld, P. E.; Henry, C. L.; Dills, R. L.; Harrison, R. B. Comparison of Odor Emissions from Three Different Biosolids Applied to Forest Soil. *Water, Air, Soil Pollut.* **2001**, *127*, 173−191.
(56) Meinardi, S.; Simpson, I. J.; Blake, N. J.; Blake, D. R.; Rowland, F. S. Dimethyl Disulfide (DMDS) and Dimethyl Sulfide (DMS) Emissions from Biomass Burning in Australia. *Geophys. Res. Lett.* **2003**, *30*, 1454.
(57) Barnes, I.; Hjorth, J.; Mihalopoulos, N. Dimethyl Sulfide and Dimethyl Sulfoxide and Their Oxidation in the Atmosphere. *Chem. Rev.* **2006**, *106*, 940−975.
(58) Berresheim, H.; Elste, T.; Tremmel, H. G.; Allen, A. G.; Hansson, H. C.; Rosman, K.; Dal Maso, M.; Mäkelä, J. M.; Kulmala, M.; O'Dowd, C. D. Gas-Aerosol Relationships of H_2SO_4, MSA, and OH: Observations in the Coastal Marine Boundary Layer at Mace Head, Ireland. *J. Geophys. Res.* **2002**, *107*, 8100.
(59) Eisele, F. L.; Tanner, D. J. Measurement of the Gas Phase Concentration of H_2SO_4 and Methane Sulfonic Acid and Estimates of H_2SO_4 Production and Loss in the Atmosphere. *J. Geophys. Res.* **1993**, *98*, 9001−9010.
(60) Perraud, V.; Horne, J. R.; Martinez, A.; Kalinowski, J.; Meinardi, S.; Dawson, M. L.; Wingen, L. M.; Dabdub, D.; Blake, D. R.; Gerber, R. B.; et al. The Future of Airborne Particles in the Absence of Fossil Fuel Sulfur Dioxide Emissions. *Proc. Natl. Acad. Sci. U. S. A.* **2015**, in press.
(61) Kreidenweis, S. M.; Seinfeld, J. H. Nucleation of Sulfuric Acid-Water and Methanesulfonic Acid-Water Solution Particles: Implications for the Atmospheric Chemistry of Organosulfur Species. *Atmos. Environ.* **1988**, *22*, 283−296.
(62) Kreidenweis, S. M.; Flagan, R. C.; Seinfeld, J. H.; Okuyama, K. Binary Nucleation of Methanesulfonic Acid and Water. *J. Aerosol Sci.* **1989**, *20*, 585−607.
(63) Wyslouzil, B. E.; Seinfeld, J. H.; Flagan, R. C.; Okuyama, K. Binary Nucleation in Acid-Water Systems. I. Methanesulfonic Acid-Water. *J. Chem. Phys.* **1991**, *94*, 6827−6841.
(64) Wyslouzil, B. E.; Seinfeld, J. H.; Flagan, R. C.; Okuyama, K. Binary Nucleation in Acid-Water systems. II. Sulfuric Acid-Water and a Comparison with Methanesulfonic Acid-Water. *J. Chem. Phys.* **1991**, *94*, 6842−6850.
(65) Dawson, M. L.; Perraud, V.; Gomez, A.; Arquero, K. D.; Ezell, M. J.; Finlayson-Pitts, B. J. Measurement of Gas-Phase Ammonia and Amines in Air by Collection onto an Ion Exchange Resin and Analysis by Ion Chromatography. *Atmos. Meas. Tech.* **2014**, *7*, 2733−2744.
(66) Grimme, S.; Antony, J.; Ehrlich, S.; Krieg, H. A consistent and Accurate Ab Initio parametrization of Density Functional Dispersion Correction (DFT-D) for the 94 Elements H-Pu. *J. Chem. Phys.* **2010**, *132*, 154104.
(67) Bork, N.; Du, L.; Reiman, H.; Kurtén, T.; Kjaergaard, H. G. Benchmarking Ab Initio Binding Energies of Hydrogen-Bonded Molecular Clusters Based on FTIR Spectroscopy. *J. Phys. Chem. A* **2014**, *118*, 5316−5322.
(68) Ahlrichs, R.; Furche, F.; Hättig, C.; Klopper, W. M.; Sierka, M.; Weigend, F. *Turbomole V6.4*, A Development of University of Karlsruhe and Forschungszentrum Karlsruhe GmbH; Turbomole GmbH, 2013.
(69) Weigend, F.; Häser, M. RI-MP2: First Derivatives and Global Consistency. *Theor. Chem. Acc.* **1997**, *97*, 331−340.
(70) Loukonen, V.; Kurten, T.; Ortega, I. K.; Vehkamaki, H.; Padua, A. A. H.; Sellegri, K.; Kulmala, M. Enhancing Effect of Dimethylamine in Sulfuric Acid Nucleation in the Presence of Water - A Computational Study. *Atmos. Chem. Phys.* **2010**, *10*, 4961−4974.
(71) Henschel, H.; Navarro, J. C. A.; Yli-Juuti, T.; Kupiainen-Määttä, O.; Olenius, T.; Ortega, I. K.; Clegg, S. L.; Kurtén, T.; Riipinen, I.; Vehkamäki, H. Hydration of Atmospherically Relevant Molecular Clusters: Computational Chemistry and Classical Thermodynamics. *J. Phys. Chem. A* **2014**, *118*, 2599−2611.
(72) Dawson, M. L.; Varner, M. E.; Perraud, V.; Ezell, M. J.; Wilson, J.; Zelenyuk, A.; Gerber, R. B.; Finlayson-Pitts, B. J. Amine−Amine Exchange in Aminium−Methanesulfonate Aerosols. *J. Phys. Chem. C* **2014**, *118*, 29431−29440.
(73) McGraw, R.; Laaksonen, A. Scaling Properties of the Critical Nucleus in Classical and Molecular-Based Theories of Vapor-Liquid Nucleation. *Phys. Rev. Lett.* **1996**, *76*, 2754−2757.
(74) Kupiainen-Määttä, O.; Olenius, T.; Korhonen, H.; Malila, J.; Dal Maso, M.; Lehtinen, K.; Vehkamäki, H. Critical Cluster Size Cannot in Practice be Determined by Slope Analysis in Atmospherically Relevant Applications. *J. Aerosol Sci.* **2014**, *77*, 127−144.
(75) Wei, C. Structure of Ammonium Methanesulfonate. *Acta Crystallogr., Sect. C: Cryst. Struct. Commun.* **1986**, *42*, 1839−1842.

DOI: 10.1021/acs.jpcb.5b07433
J. Phys. Chem. B 2016, 120, 1526−1536